Suboptimal MPC-based spacecraft attitude control with reaction wheel desaturation

Miguel Castroviejo-Fernandez¹, Jordan Leung¹ and Ilya Kolmanovsky¹

Abstract—A Time-Distributed Model Predictive Control (TDMPC) is applied to spacecraft attitude stabilization in the Local Vertical Local Horizontal (LVLH) frame with concurrent reaction wheel desaturation. This is accomplished without using thrusters, i.e., with zero fuel consumption, and exploiting gravity gradient torques. The TDMPC uses a warm-start, and a fixed number of iterations of an optimization algorithm is performed per time step to generate a suboptimal solution. An analytical estimate of the minimum number of iterations required to achieve closed-loop stability is compared to empirical estimates determined through simulations. It is shown that a small number of iterations is sufficient to perform reaction wheel desaturation maneuvers. Procedures for estimating the closed-loop regions of attraction of TDMPC are illustrated for this system.

I. INTRODUCTION

The paper considers an application of suboptimal Model Predictive Control (MPC) that we refer to, following [1], as Time Distributed MPC (TDMPC), to spacecraft attitude stabilization with concurrent desaturation of reaction wheels. Many spacecraft use reaction wheels to maintain pointing and for reorientation. Due to external moments acting on the spacecraft over long periods of time, that change the spacecraft total angular momentum, reaction wheels can spin up and eventually need to be desaturated. Traditionally, spacecraft reaction wheel desaturation is performed using thrusters to produce moments that result in the decrease of reaction wheel (RW) rotational speed. Unfortunately, thrusters consume fuel, a limited resource that constrains spacecraft operational life.

Alternative approaches (see e.g., [2]) for reaction wheel desaturation include exploiting gravity gradients (moments due to nonuniform gravity force distribution along the body of the spacecraft). With this approach, the reaction wheel desaturation can be performed without the use of thrusters and with zero fuel consumption. This is the approach considered in this paper.

As control moments that can be applied to the spacecraft by either thrusters or momentum exchange devices are limited, and there could be exclusion zones for spacecraft pointing, the use of MPC [3] is appealing for spacecraft attitude control, see e.g., [4]. In [5], MPC was exploited for reaction wheel desaturation using either gravity gradient or magnetic torques while maintaining spacecraft attitude deviation within the prescribed range.

¹University of Michigan, Ann Arbor, MI 48109 USA mcastrov, jmleung, ilya@umich.edu. This research is supported by Air Force Office of Scientific Research Grant number FA9550-20-1-0385 and National Science Foundation award CMMI-1904394

Suboptimal MPC strategies, in which the exact solution to the finite horizon optimal control problem is replaced by an approximate one which is easier to compute is of interest for spacecrafts for which the onboard computing capabilities are limited. Limitations may originate due to the use of slow radiation-hardened processors, small size of the spacecraft (CubeSat or SmallSat) or due to the need to reduce electrical power consumption which depends on solar panels for regeneration.

In TDMPC [1] and real-time iterations [6], a suboptimal solution to the MPC problem is generated through the use, at each time step, of a few iterations of an optimizer and warm-starting. Such a suboptimal MPC can be viewed as a dynamic controller with the controller states corresponding to the solution estimate which is updated by a few iterations of the optimizer applied, at every time step, to the optimal control problem parameterized by the system state at that time instant. Closed-loop stability guarantees can then be obtained if a sufficient number of iterations is performed by the optimizer at every time step using, for instance, the small gain theorem-based analysis [1]. In [7], [8], analytical methods to estimate the minimum number of iterations per time step l^* and generate estimates of closed-loop region of attraction (RoA) have been developed for the case of linear quadratic MPC (LQ-MPC) with input constraints and a primal projected gradient optimizer.

The contributions of this paper are as follows. Firstly, we demonstrate the application of TDMPC to simultaneous spacecraft attitude stabilization and reaction wheel desaturation. It is shown that TDMPC can stabilize spacecraft pointing in Local Vertical Local Horizontal (LVLH) plane while reaction wheels angular momenta and their rotation speeds are reduced. Secondly, for the case of primal projected gradient optimizer used in TDMPC, we compute and compare the analytical and empirical estimates l^* and closedloop RoAs for different prediction horizon lengths. It is shown that the reaction wheel desaturation objectives for the spacecraft with control constraints can be achieved with the short horizon LQ-MPC and with the primal projected gradient optimizer that uses a very small number of iterations per time step. Even though LQ-MPC uses a linear model for prediction, these conclusions are verified in simulations on the nonlinear spacecraft model. Thirdly, we illustrate the possibility of (conservatively) handling state constraints on spacecraft pointing attitude by "scaling" the invariant closedloop RoAs.

We note that in the case of control input constraints, a saturated LQR control, for which closed-loop RoAs can be

estimated, also provides a computationally efficient solution to the problem. At the same time, MPC, which is aware of the constraints over the prediction horizon, generally provides better responses without oscillations and with shorter settling time. Furthermore, MPC is able to simultaneously handle state constraints. Explicit MPC [9] provides a computationally efficient solution for low dimensional problems; however, in the case of spacecraft attitude control with reaction wheel desaturation the problem is already medium-size, and it is unclear if sufficient symmetries exist for the spacecraft dynamics in LVLH frame that can be effectively exploited for the dimensionality reduction (e.g., yaw and roll dynamics are inherently coupled). Thus, we believe TDMPC provides a suitable choice for the system considered.

The paper is organized as follows. We start with the model in Section II for the spacecraft three-dimensional (yaw-pitch-roll) attitude dynamics, and we also include a lower dimensional model for the pitch only dynamics. In Section III, we review TDMPC and discuss procedures to estimate l^* and RoAs. We illustrate the application to spacecraft attitude control with reaction wheel desaturation in Section IV. Finally, in Section V concluding remarks and directions for future work are summarized.

Notations: Let \mathbb{S}^n_{++} , \mathbb{S}^n_+ denote the set of symmetric $n \times n$ positive definite and positive semidefinite matrices respectively. I_m denotes the $m \times m$ identity matrix. Given $W,\ M \in \mathbb{S}^n_{++},\ \lambda_W^-(M),\ \lambda_W^+(M)$ denote the minimum and maximum eigenvalues of $\sqrt{W}^{-1}M\sqrt{W}^{-1}$. Given $x \in \mathbb{R}^n$ and $W \in \mathbb{S}^n_+$, the W-norm of x is $||x||_W = \sqrt{x^\top W x}$. Given $P \in \mathbb{S}^n_{++},\ \mathcal{B}_P(r) = \{x \in \mathbb{R}^n \mid ||x||_P \leq r\}$. Let $c(\cdot) = \cos(\cdot),\ s(\cdot) = \sin(\cdot)$.

II. PROBLEM SETTING

In this paper, we consider a spacecraft in circular motion around a celestial body. The spacecraft is equipped with a Reaction Wheel Array (RWA) that consists of three reaction wheels, each along the corresponding principal axis of the spacecraft. An extension to a RWA with 4 reaction wheels will be addressed in future publications. The case of small orbital radius is particularly relevant as the gravity gradients effect is stronger. Note that, depending on the setting, other external disturbances, such as drag, magnetic moments, solar radiation pressure might affect the spacecraft dynamics.

A. Gravity gradients

Gravity gradients are torques that appear on an object in a gravitational field due to the fact that the gravitational force decreases with the square of the distance. As a result, a spacecraft orbiting around a celestial body will have a weaker pull on the parts it has further away from the body. As the gravity gradient torque is an external torque, it is able to change the total angular momentum of the spacecraft and hence reduce reaction wheel angular momentum while maintaining spacecraft pointing.

B. Model

Let \mathcal{I} be an inertial frame, \mathcal{S} be a body fixed frame aligned with the principal axes of the spacecraft and \mathcal{G} be a Local Vertical Local Horizontal (LVLH) frame as described in [10].

The orientation of the body fixed frame \mathcal{S} with respect to LVLH frame \mathcal{G} is specified by 3-2-1 Euler yaw-pitch-roll angles, ψ , θ , ϕ . The angular velocity of spacecraft body fixed frame with respect to the inertial frame is given by $\vec{\omega}_{\mathcal{S}/\mathcal{I}}|_{\mathcal{S}} = \begin{bmatrix} \omega_1 & \omega_2 & \omega_3 \end{bmatrix}^{\top}$. Then, following [10]:

$$\begin{bmatrix} \dot{\phi} \\ \dot{\theta} \\ \dot{\psi} \end{bmatrix} = \frac{1}{c(\theta)} \begin{bmatrix} c(\theta) & s(\phi)s(\theta) & c(\phi)s(\theta) \\ 0 & c(\phi)c(\theta) & -s(\phi)c(\theta) \\ 0 & s(\phi) & c(\phi) \end{bmatrix} \begin{pmatrix} \begin{bmatrix} \omega_1 \\ \omega_2 \\ \omega_3 \end{bmatrix} + \\ n \begin{bmatrix} c(\theta)s(\psi) \\ s(\phi)s(\theta)s(\psi) + c(\phi)c(\psi) \\ c(\phi)s(\theta)s(\psi) - s(\phi)c(\psi) \end{bmatrix} \end{pmatrix}, \tag{1}$$

 $n=\sqrt{\frac{\mu}{r_0^3}}$ is the circular orbit gravitational parameter. The Euler's equations for the evolution of the angular velocity are given by

$$\begin{bmatrix} J_1 \dot{\omega}_1 \\ J_2 \dot{\omega}_2 \\ J_3 \dot{\omega}_3 \end{bmatrix} = \begin{bmatrix} (J_2 - J_3)(\omega_2 \omega_3 - 3n^2 C_{23} C_{33}) \\ (J_3 - J_1)(\omega_1 \omega_3 - 3n^2 C_{13} C_{33}) \\ (J_1 - J_2)(\omega_1 \omega_2 - 3n^2 C_{13} C_{23}) \end{bmatrix} + \begin{bmatrix} M_1 \\ M_2 \\ M_3 \end{bmatrix}.$$
(2)

Here $C_{13}=-s(\theta)$, $C_{23}=s(\phi)c(\theta)$, $C_{33}=c(\phi)c(\theta)$, J_1 , J_2 , J_3 are the principal moments of inertia and M_k^i , k=1,2,3, are the moments produced by the RWs.

The angular momentum of the k^{th} reaction wheel is given by $h_k = J_k^{RW}(\omega_k + \Omega_k), \ k = 1, \dots, 3$, where Ω_k [rad/s] is the rotational speed of the corresponding reaction wheel. The evolution of the reaction wheel angular momenta is given by

$$\begin{bmatrix} \dot{h}_1 \\ \dot{h}_2 \\ \dot{h}_3 \end{bmatrix} = \begin{bmatrix} 0 & \omega_3 & -\omega_2 \\ -\omega_3 & 0 & \omega_1 \\ \omega_2 & -\omega_1 & 0 \end{bmatrix} \begin{bmatrix} h_1 \\ h_2 \\ h_3 \end{bmatrix} - \begin{bmatrix} M_1 \\ M_2 \\ M_3 \end{bmatrix} . (3)$$

The equations of motion (1)-(3) can be aggregated into,

$$\dot{x} = f(x, u),\tag{4}$$

with the state of the system x defined as

$$x = [\phi, \ \theta, \ \psi, \ \omega_1, \ \omega_2, \ \omega_3, \ h_1, \ h_2, \ h_3]^\top,$$

and with the control input given by

$$u = [M_1, M_2, M_3]^{\top}.$$

The control inputs are subject to saturation constraints:

$$u \in \mathcal{U}$$
.

where the set \mathcal{U} is a hyper-rectangle.

In the subsequent simulations, we consider a spacecraft on ciruclar orbit around a body with $\mu=3.986\times 10^5~[\mathrm{km^3\cdot s^{-2}}]$, at an altitude of 500 [km] $(n=1.1086\times 10^{-3}~[\mathrm{s^{-1}}])$ and an orbital period $T_{orb}=\frac{2\pi}{n}\approx 1.58~\mathrm{hr}$. The moment of inertia are $J_1=1000,~J_2=2200,~J_3=1400~[\mathrm{kg\cdot m^2}].$

C. Reduced order model for pitch-only dynamics

The pitch-only dynamics of the spacecraft are of interest as they can be analyzed more easily, using a lower-dimensional model. By setting

$$\phi = \psi = \omega_1 = \omega_3 = h_1 = h_3 = 0, \tag{5}$$

in (1), (2) and (3) and defining $x = \begin{bmatrix} \theta & \omega_2 & h_2 \end{bmatrix}^T$, the pitch-only dynamics can be represented by

$$\dot{x} = \begin{bmatrix} \dot{\theta} \\ \dot{\omega}_2 \\ \dot{h}_2 \end{bmatrix} = \begin{bmatrix} \omega_2 + n \\ (J_3 - J_1) \frac{3n^2 s(\theta)c(\theta)}{J_2} + \frac{u_2}{J_2} \\ -u_2 \end{bmatrix} , \quad (6)$$

$$u_2 = M_2. (7)$$

Note that, for system (4), the set $\{x: \phi = \psi = \omega_1 = \omega_3 = h_1 = h_3 = 0\}$ is forward invariant if $u_1 = u_3 = 0$; hence any trajectory starting in this set and with no torques applied to yaw and roll RWs evolves in a lower dimensional manifold actually represented by the pitch-only model (6)-(7).

D. Equilibria, linearization and control model

Table I shows the state values at different unforced equilibria of the spacecraft model. All the equilibria presented correspond to standard spacecraft attitude configurations, and are parameterized by n, the angular velocity of $\mathcal G$ with respect to $\mathcal I$. Note that depending on the spacecraft orientation at a particular equilibrium, the angular momentum of one of the reaction wheels aligned with the axis of orbital rotation can be arbitrarily set, while the other two reaction wheels have zero angular momentum.

TABLE I: State values at different unforced equilibria. $h_{\rm eq}$ is a free variable.

By the definition of the LVLH frame, the normal to the orbital plane is along the second unit vector of the frame. Because of this, $x_{0,2}$ and $x_{0,3}$ - both equilibria assume that the orbital rotation takes place along a different unit vector - are not physically relevant. Therefore simulations of the spacecraft will aim to bring the state to $x_{0,1}$. The equilibrium $x_{0,1}$ also corresponds to an equilibrium for the spacecraft model with the pitch only dynamics. For the numerical parameters given, this equilibrium is open-loop unstable.

With the nonlinear model in the form (4), the linearized spacecraft model is given by:

$$\Delta \dot{x}(t) = A_c \Delta x(t) + B_c u(t), \tag{8}$$

where $\Delta x = x - x_{0,1}$, $A_{c,i,j} = \frac{\partial f_i}{\partial x_j}$ and $B_{c,i,j} = \frac{\partial f_i}{\partial u_j}$. A linear discrete-time model that is used for prediction in MPC can then be obtained using the Zero-order hold approximation and has the form,

$$\Delta x_{k+1} = A\Delta x_k + B\Delta u_k \ . \tag{9}$$

In the subsequent simulations, discretization of the spacecraft model is made using a sampling period of Ts = 2 [s].

III. TDMPC DESIGN AND ANALYSIS

In this section, we first describe a general LQ-MPC problem. We then consider TDMPC and, finally, discuss RoA estimation

A. Model Predictive Control

For a linear discrete-time prediction model with input constraints,

$$x_{k+1} = Ax_k + Bu_k, (10)$$

$$u \in \mathcal{U}, \quad x_0 = x^0, \tag{11}$$

where $x \in \mathbb{R}^n$, $u \in \mathbb{R}^m$, $A \in \mathbb{R}^{n \times n}$, $B \in \mathbb{R}^{n \times m}$, LQ-MPC determines the control action by solving the following Optimal Control Problem (OCP),

$$\min_{\xi,\nu} \quad \|\xi_N\|_P^2 + \sum_{i=0}^{N-1} \|\xi_i\|_Q^2 + \|\nu_i\|_R^2$$
 (12)

s f

$$\xi_{i+1} = A\xi_i + B\nu_i, \quad i = 0, \dots, N-1,$$
 (13)

$$\xi_0 = x, \quad \nu_i \in \mathcal{U}, \quad i = 0, \dots, N - 1.$$
 (14)

Where $N \in \mathbb{N}$ is the prediction horizon length, $Q \in \mathbb{R}^{n \times n}$, $R \in \mathbb{R}^{m \times m}$ and $P \in \mathbb{R}^{n \times n}$ are weighting matrices, and x is the current state. The optimal solution to the OCP (12)-(14) for $\xi_0 = x$ is given by $\xi^*(x) = (\xi_0^*, \dots, \xi_N^*)$ and $\nu^*(x) = (\nu_0^*, \dots, \nu_{N_1}^*)$. The control input at the time instant k is defined as $u_k = \nu_0^*(x_k)$, Where $\nu_0^*(x_k)$ is the first element of the sequence $\nu^*(x)$. At the next time step, the state x_{k+1} is measured, the OCP with $\xi_0 = x_{k+1}$ is solved and the next control action is computed.

Following [7], the following assumptions ensure that the MPC feedback law is stabilizing:

Assumption 1: The pair (A, B) is stabilizable. $Q \in \mathbb{S}_+^n$, $R \in \mathbb{S}_{++}^n$ and P satisfies the associated Discrete Algebraic Riccati Equation (DARE).

Assumption 2: \mathcal{U} is closed, convex and contains the origin in its interior.

The OCP (12)-(14) can be rewritten in condensed form:

$$\min_{z \in \mathcal{Z}} \quad J(x, z) = \left\| \begin{bmatrix} x \\ z \end{bmatrix} \right\|_{\mathcal{M}}^{2} \tag{15}$$

where $z = \begin{bmatrix} \nu_0^\top & \dots & \nu_N^\top \end{bmatrix}^\top \in \mathbb{R}^{mN}$ and

$$\mathcal{Z} = \mathcal{U}^N, \quad \mathcal{M} = \begin{bmatrix} H & G \\ G^\top & W \end{bmatrix}.$$
 (16)

The expressions to compute matrices H, G, W are given in [7]. If $z^*(x)$ is the optimal solution of (15), then the MPC control law is given by

$$u_k = \Xi z^*(x_k), \quad \Xi \equiv \begin{bmatrix} I_{m \times m} & 0_{m \times m(N-1)} \end{bmatrix}.$$
 (17)

Additionally, the value function

$$V(x) = \left\| \begin{bmatrix} x \\ z^* \end{bmatrix} \right\|_{M}^{2}, \tag{18}$$

representing the optimal cost for a given x, serves as a Lyapunov function for the closed loop system under the optimal MPC feedback law, [11], [12].

B. Time Distributed MPC

Usually, (15) is solved by an iterative algorithm. Let us denote by $\mathcal{T}^l:\mathbb{R}^n\times\mathbb{R}^{mN}\to\mathbb{R}^{mN}$ the mapping from a starting (x,z) pair to the output of the algorithm after $l\in\mathbb{N}$ iterations. Due to computational limitations, it is often not possible to compute the optimal solution of (15) exactly; hence a suboptimal approximation must be used. For the TDMPC scheme studied in [8], the suboptimal solution at time instant k is obtained by updating the solution computed at the previous time-step, k-1, through a fixed number of primal Projected Gradient (PG) iterations:

$$\mathcal{T}_{PGM}(x,z) = \Pi_{\mathcal{Z}}[z - \alpha \nabla_z J(x,z)], \tag{19}$$

$$\mathcal{T}^{l}(x,z) = \mathcal{T}_{PGM}(\mathcal{T}^{l-1}(x,z),x), \tag{20}$$

where $\mathcal{T}^0(x,z)=z$, $\Pi_{\mathcal{Z}}$ is the Euclidean projection onto \mathcal{Z} . and $\alpha=2/(\lambda^+(H))+\lambda^-(H))$ is the optimal step length, as described in [7]. Given that, for the spacecraft, \mathcal{U} is a box the projection operation is easy to compute.

The plant-optimizer system is then given by:

$$x_{k+1} = Ax_k + B\Xi z_k \tag{21}$$

$$z_k = \mathcal{T}^l(x_k, z_{k-1}). \tag{22}$$

Under Assumptions 1-2, [8, Lemma 9] states that if $l > l^*$ iterations are performed then there exists a set $\Sigma \subseteq \mathbb{R}^n \times \mathbb{R}^{mN}$ that is forward invariant under the closed loop dynamics. The procedure to compute l^* in closed-form as a function of the problem data is described in [8]. Additionally, under the same assumptions and performing $l > l^*$ iterations, [8, Theorem 4] states that the origin of the plant-optimizer system is asymptotically stable (AS) with a forward invariant RoA estimate Σ .

C. RoA estimates

The aforementioned set Σ is defined, from [8], as:

$$\Sigma = \{ (x, z) \in \Gamma_N \times \mathcal{Z} \mid \phi(x, z) \le r_\phi \}, \qquad (23)$$

$$\Gamma_N = \left\{ x \in \mathbb{R}^n \mid \psi(x) < r_{\psi} \right\},\tag{24}$$

where $\psi(x) = \sqrt{V(x)}$ is the square root of the value function defined in (18), while $\phi(x,z) = \|z - z^*(x)\|$ is the error between z and the solution of (15) for x. Values of r_{ψ} , r_{ϕ} can be found in [8]. Finally, note that Γ_{N} is a sublevel set of the value function introduced by [12, Theorem 1]. All level sets of $V(\cdot)$ that are contained in Γ_{N} are forward invariant for the corresponding system, as shown in [8, Corollary 2].

Note that Γ_N and $\phi(x,z)$ depend, on the optimal MPC solution $z^*(x)$ and hence it is not possible to check online/in real-time, if $(x,z)\in \Sigma$ without losing the computational advantages of the TDMPC. To circumvent this issue in [8, section V-A] two subsets of Γ_N are introduced. The first subset, \mathcal{H}_N , is a polytopic approximation of Γ_N obtained by sampling, offline, a certain number of points $x\in \Gamma_N$ and computing the associated convex hull. This set, \mathcal{H}_N , can approximate Γ_N with arbitrary precision given that enough points are considered in the offline computations. The second

subset provides a more conservative approximation but does not require offline sampling, and is defined as

$$\mathcal{B}_W(r_{\psi}) = \{ x \in \mathbb{R}^n \mid ||x||_W \le r_{\psi} \}. \tag{25}$$

In addition, a sufficient condition to ensure that $\phi(x_k, z_k) \le r_{\phi}$ is given in [8, section V-B]. It should be noted that all the RoA estimates presented in this section are for the controller applied to (10)-(11).

IV. CASE STUDIES

A. Nominal control constraints and controller

The weighting matrices in (12) for the nominal controller and full order spacecraft model are chosen as diag([.1, .1, .1, .01, .01, .01, .001, .001, .001]), Q $R = \text{diag}([5000 \ 5000 \ 5000])$, and P is chosen as the solution of the associated Discrete Algebraic Riccati Equation (DARE). The control constraints represent the maximum torque limit: $abs(M_i) \le 0.08 [N \cdot m], j = 1, 2, 3$. The horizon N is chosen as N=25 steps. Assumptions 1 and 2 hold for the discretized linearized model of spacecraft dynamics with these constraints. For the reduced order pitchonly model the weights are chosen from the above Q an Rmatrices associated with variables retained in the reduced order model. In this paper, OCPs for LQ-MPC controllers are solved using the quadprog() function from Matlab using an interior-point algorithm[13].

Table II shows the analytical estimate of l^* along with an empirical estimate l_{min} of the necessary number of iterations to maintain closed-loop asymptotic stability and convergence properties similar to $l = l^*$. To estimate l_{min} we used simulations of the controller in the loop with the discretetime linearized model and with 100 randomly selected initial conditions. The value of l_{min} was the smallest value of l for which the state and control vector deviated from zero by less than a specified threshold $(10^{-3}, 10^{-5})$ respectively) in norm over the last 20% of the simulation time (10 orbits) for all 100 initial conditions, and the same also held for l+1, l+2, l+3 and l+4 iterations per time step. We confirmed that these properties also held for $l = l^*$. The selected threshold was found empirically to adequately assess the convergence of the simulations. As Table II indicates, one iteration per time step of TDMPC is sufficient based on simulations, and seven iterations per time step are sufficient based on the theoretical guarantees in [8].

$$\begin{array}{c|cccc} & l^* & l_{\min} \\ \hline \text{spacecraft dynamics} & 7 & 1 \\ \text{pitch-only dynamics} & 7 & 1 \\ \end{array}$$

TABLE II: Estimated minimal number of iterations l^* per [8, Lemma 9] and the minimum number of iterations based on simulations required to achieve closed-loop stability.

Figures 1, 2 compare the spacecraft desaturation maneuvers using MPC (exact solution) and TDMPC with l=1 with the reduced order pitch-only nonlinear model and full order nonlinear model, respectively. For the pitch-only closed-loop simulations (Figure 1), the initial value of RW

angular momentum is $h_2(0) = 10 \ [\mathbb{N} \cdot \mathbb{m} \cdot \mathbb{s}]$ and $\theta(0) = 0$. The controllers tilt the spacecraft, with θ reaching values around $-0.6 \ [\text{rad}]$. Note that to maintain the spacecraft tilted the RW has to maintain a non-zero angular acceleration and by this process the angular momentum of the RW is reduced. The RW is desaturated and the original attitude is regained in about 6 orbits. Figure 2 shows simulations with the full order nonlinear model for the initial RW angular momenta given by $[h_1,\ h_2,\ h_3]^\top = [5,10,5]^\top \ [\mathbb{N} \cdot \mathbb{m} \cdot \mathbb{s}]$. The bottom graph of Figure 2 shows the inputs to the system. Note that the control limits are not reached in this simulation and no apparent differences are seen between MPC and TDMPC with l=1.

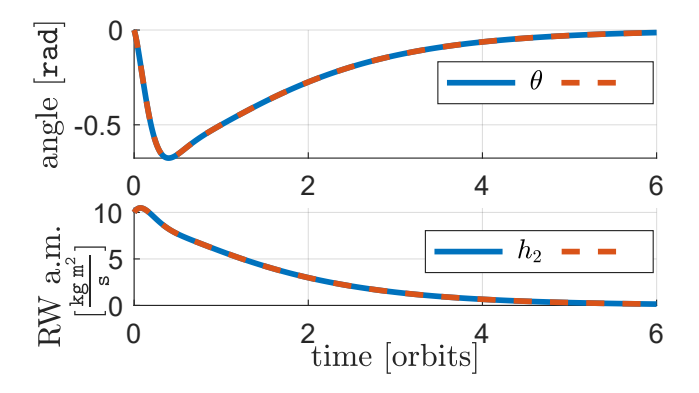


Fig. 1: State evolution for the pitch-only dynamics desaturation maneuver in two cases: using MPC (solid lines) and using a TDMPC with 1 iteration per time step (dashed lines).

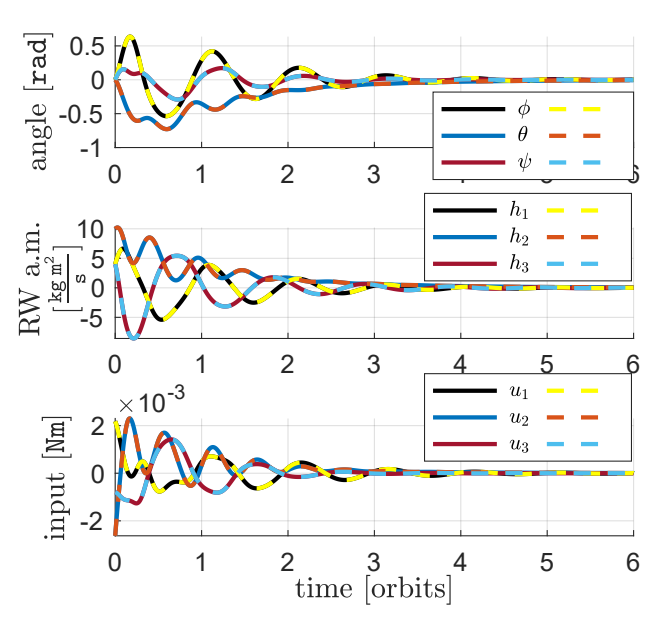


Fig. 2: State and input evolution for the spacecraft desaturation maneuver with the full order model in two cases: using MPC (solid lines) and using TDMPC with 1 iteration per time step (dashed lines).

B. Tighter control constraints and more aggressive controller

We next modify the control constraints and weights as follows:

$$|u_1| \le 0.04, \quad |u_2| \le 0.04, \quad |u_3| \le 0.04, \quad (26)$$

$$Q_a = \text{diag}([.1 .1 .1 .01 .01 .01 .1 .1 .1]),$$
 (27)

$$R_a = \text{diag}([50 \ 50 \ 50]).$$
 (28)

The combined effect of tighter control constraints and a more aggressive controller is that control constraint activation in desaturation maneuvers becomes more likely. The required number of iterations in this case is $l^{\ast}=66,\ l_{\min}=1,$ for both the reduced order and full order spacecraft dynamics. Compared to the nominal case in Section IV-A, the analytically computed value of l^{\ast} has increased while l_{\min} has not changed. This suggests that the analytically computed estimate becomes more conservative with tighter control constraints.

Figure 3 shows the state/input evolution starting from $h_2(0)=1$ [N·m·s] for the pitch-only nonlinear model of spacecraft dynamics and controllers based on (26)-(28). The closed-loop response with TDMPC and l^* iterations is very close to that of the exact MPC, however, the TDMPC with l_{min} iterations shows oscillations during the first 10 steps.

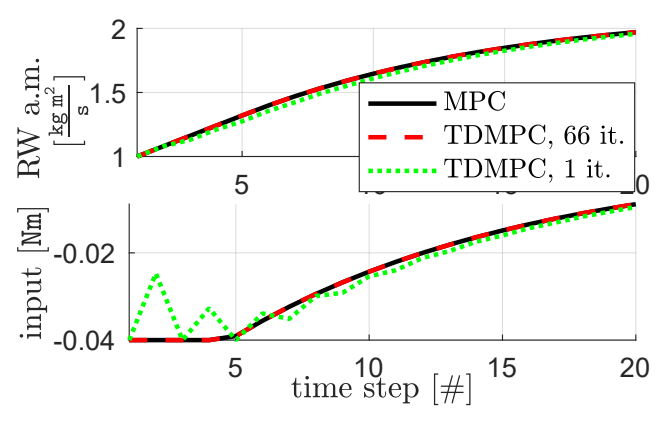


Fig. 3: State and input evolution for the desaturation of the pitch-only dynamics with controllers based on (26)-(28). Simulations show the nonlinear system controlled by: a MPC (solid black lines), a TDMPC with $l^* = 66$ iterations (dashed red lines), a TDMPC with $l^* = 1$ iterations (dotted green lines). Convergence to the origin is observed in approximately 3 orbits (not shown).

C. Differences between MPC and TDMPC

In order to further characterize the discrepancy between optimal and suboptimal trajectories, we run simulations, for the pitch-only dynamics, with MPC and with TDMPC performing l_{\min} or l^* iterations.

Both the nominal weight and constraint choices in Section IV-A and the modified ones in Section IV-B are considered resulting in 4 controller choices, respectively: $TDMPC_{1,l}$, MPC_1 , $TDMPC_{2,l}$, MPC_2 .

For each controller the same 100 initial conditions are simulated. Those are taken from a uniform distribution with $\theta \in [-1 \ 1], \ \omega_2 \in [-2n \ 2n], \ h_2 \in [-20 \ 20].$ We use

$$e_{\text{TDMPC}_{i,l}}(t) = \log_{10} \left(\left\| \begin{bmatrix} x_{\text{TDMPC}_{i,l}}(t) \\ u_{\text{TDMPC}_{i,l}}(t) \end{bmatrix} - \begin{bmatrix} x_{\text{MPC}_{i}}(t) \\ u_{\text{MPC}_{i}}(t) \end{bmatrix} \right\| \right),$$
(29)

where i=1,2 for the error characterization. Figure 4 shows median, mean, lower and upper quartile as well as minimum and maximum values of the maximum error of states and inputs of $\max(e_{\mathrm{TDMPC}_{i,l}})$. The maximum value of the error occurs, in most cases, within the first 0.1 [orbit]. When considering l^* iterations, both TDMPC_{1,l^*} and TDMPC_{2,l^*} give small deviation values, median maximum error being around 10^{-5} and 10^{-4} respectively. When considering $\mathrm{TDMPC}_{1,l_{\min}}$ and $\mathrm{TDMPC}_{2,l_{\min}}$ the difference between medians reaches values of around $10^{-2.5}$ and 10^{-2} respectively. The increase in the error that occurs for the case of tighter constraints and more aggressive weights is attributed to the underlying OCP becoming harder to solve so that the accuracy obtained with a single iteration is reduced.

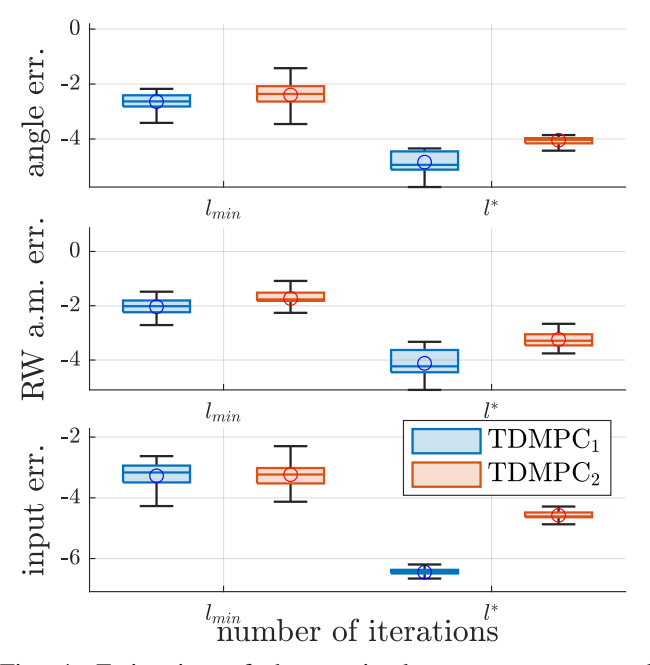


Fig. 4: Estimation of the maximal error on states and inputs, as described by (29), i.e. error with respect to the regular MPC solution. Errors are presented for two TDMPC controllers differing by the number of iterations performed. Boxes represent the lower and upper quartiles. The line within the box is the median value. The round marker shows the mean value. The horizontal bars at the end of the whiskers, the minimum and maximum values.

D. RoA Estimation

Figure 5 (left) show 2D projections of the set Γ_N in (24) for the pitch-only model and nominal weights/control constraints (Section IV-A). On the same figures, RoA estimates \mathcal{H}_N (Section III-C) and $\mathcal{B}_W(r_\psi)$ (see (25)) are also shown. The sublevel set-based estimate, $\mathcal{B}_W(r_\psi)$, of RoA is

a fairly accurate approximation of Γ_N . Also, as the polytopic approximation \mathcal{H}_N can be refined to an arbitrary degree the set Γ_N and \mathcal{H}_N overlap almost completely. Due to overlapping of the sets, colors in Figures 5-6 differ from their legends: dark orange at the intersection of the three sets and purple at $\mathcal{H}_N \cap \Gamma_N$.

Similarly, Figure 5 (right) shows 2D sections of the RoA estimates for the full-order model of the spacecraft. The sections, along θ , ω_2 , h_2 , match closely those for the pitch-only dynamics. Note that desaturation of up to $30 \, [\text{N} \cdot \text{m} \cdot \text{s}]$ is possible provided the spacecraft angular velocity is not too large (e.g. up to $7n \approx 0.074 \, [\text{rpm}]$ is permissible).

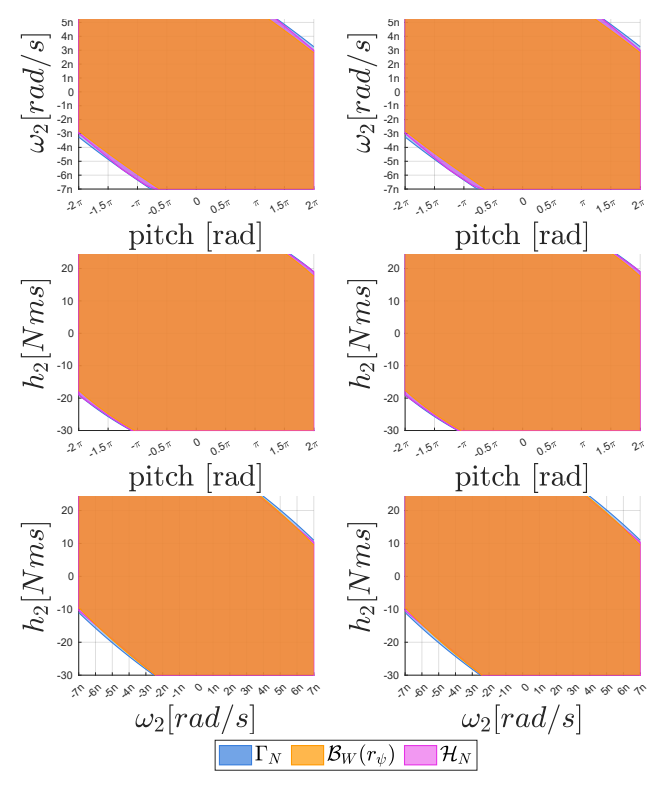


Fig. 5: 2D section of the RoA estimates Γ_N (blue), \mathcal{H}_N (pink), $\mathcal{B}_W(r_\psi)$ (orange) for the TDMPC controlled pitchonly model (left) and spacecraft model (right). 2D section along pitch angle, ω_2 , h_2 .

The conservatism of the sublevel-set approximation, $\mathcal{B}_W(r_\psi)$ depends on the prediction horizon, N. Figure 6 shows the same sections as in Figure 5 (upper row) for N=125 (left) and N=625 (right). While Γ_N grows monotonically with N [12] (although no perceivable change can be seen here), $B_W(r_\psi)$ progressively shrinks as N increases. Considering that

$$\mathcal{B}_{W}(r_{\psi}) = \{ x \in \mathbb{R}^{n} \mid ||x||_{W} \le r_{\psi} \},$$

$$\lambda_{I_{n}}^{-}(W) ||x||_{I_{n}}^{2} \le ||x||_{W}^{2},$$
(30)

as well as the values of $\lambda_{I_n}^-(W)$, r_{ψ} in Table III it is not surprising that the set $\mathcal{B}_W(r_{\psi})$ is reduced as N increases.

Another way to see this is by noting that

$$W = Q + \begin{bmatrix} I A \dots A^N \end{bmatrix} \begin{bmatrix} I_N \otimes Q & 0 \\ 0 & P \end{bmatrix} \begin{bmatrix} I A \dots A^N \end{bmatrix}^\top,$$
(31)

where $C\otimes D\in\mathbb{R}^{pm\times qn}$ denotes the Kronecker product between matrices $C\in\mathbb{R}^{p\times q}$ and $D\in\mathbb{R}^{m\times n}$. As the system is open-loop unstable, the matrix A possesses eigenvalues outside the unit circle. Therefore, some eigenvalues of A^N grow larger in magnitude with N and hence it is expected that the norm $\|x\|_W$ increases with N. This, combined with the values of r_ψ in Table III showing little variation leads to the deterioration of the sublevel set estimate.

N	l^*	$l_{ t min}$	$\lambda_I^-(W)$	r_{ψ}
25	7	1	1.7	$1.07 \cdot 10^{-9}$
125	16	1	1.93	$5.79 \cdot 10^{-10}$
625	225	1	2.91	$3.15 \cdot 10^{-11}$

TABLE III: Values of l^* , l_{\min} , $\lambda_I^-(W)$, r_{ψ} for $N=\{25,\ 125,\ 625\}$

Table III also shows that while l^* increases with N, l_{\min} does not change.

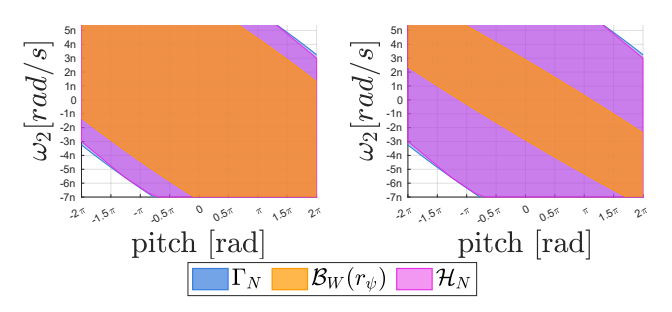


Fig. 6: θ - ω_2 section of the RoA estimates Γ_N (blue), \mathcal{H}_N (pink), $\mathcal{B}_W(r_\psi)$ (orange) for the TDMPC controlled spacecraft. Considering N=125 (left) and N=625 (right).

E. State Constraints

During the reaction wheel desaturation, the orientation of the spacecraft may need to be maintained within the prescribed range for pointing, communication or attitude exclusion zone avoidance. To address such state constraints, sublevel sets of Γ_N defined as

$$\Gamma_{N,\alpha} = \{ x \in \mathbb{R}^n \mid \psi(x) \le \alpha r_{\psi} \}, \quad 0 < \alpha \le 1,$$
 (32)

are useful. Such subsets are forward invariant provided $l > l^*$; hence if α is chosen such that $\Gamma_{N,\alpha}$ is state constraint admissible, any initial state in $\Gamma_{N,\alpha}$ will result in RW desaturation without violation of state constraints.

As an example, assume state constraints given by

$$\phi \in \begin{bmatrix} -.4 & .4 \end{bmatrix}, \; \theta \in \begin{bmatrix} -.4 & .4 \end{bmatrix}, \; \psi \in \begin{bmatrix} -.4 & .4 \end{bmatrix},$$

which can be written concisely as $x \in \mathcal{X}$. Using the procedure in [14, Proposition S1] for TDMPC with weights and control constraints from Section IV-A the value $\alpha^* = 0.0201$ was computed, for which $\Gamma_{N,\alpha^*} \subseteq \mathcal{X}$ [8, Section V-A].

Figure 7 shows several 2D projections of Γ_{N,α^*} as well as the same sections of Γ_N . Looking at the h_1 - h_3 projection, for example, we see the set Γ_{N,α^*} is much smaller (about 1/30) than Γ_N .

Figure shows the closed-loop response for the full order model with x(0) $\begin{bmatrix} 0 & 0 & 0 & n/2 & -n/4 & n/2 & 1 & 0.85 & 1 \end{bmatrix}^\top$ $\in \Gamma_{\mathcal{X},\alpha^*}$. As expected, the state constraints are satisfied. However and due to the conservatism of the method, even though we chose an initial state close to the boundary of Γ_{N,α^*} the states do not come close to the constraints, e.g., the maximum absolute value of the angle deviations is 0.2 [rad], a half of the maximum permissible value.

For the reduced order model of pitch-only dynamics the small size of Γ_{N,α^*} in $h_1,\,h_2,\,h_3$ direction can be mitigated by integrating Γ_{N,α^*} into a scheme that gradually decreases the target value of h_2 rather than setting it to zero; however, similar strategies for the full order model are less clear as values of h_1 and h_3 can only be zero at equilibria.

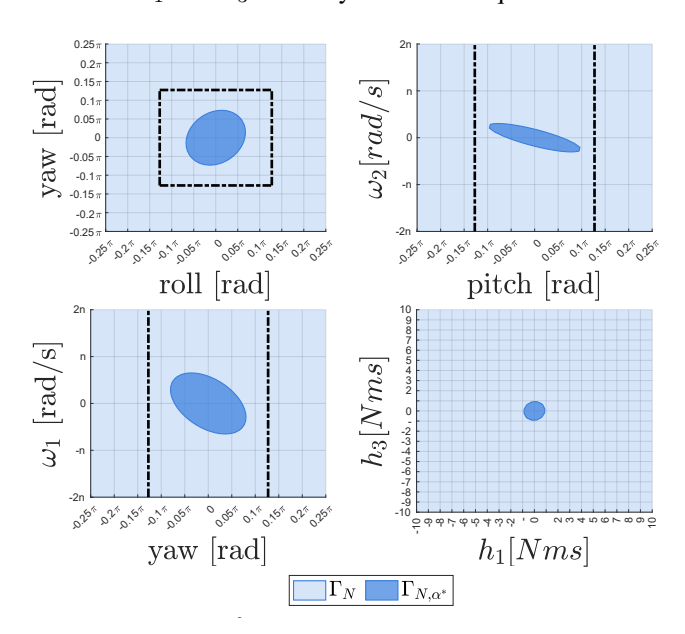


Fig. 7: Different 2D sections of the Γ_{N,α^*} set for the full order nonlinear model of spacecraft dynamics. State constraints appear, on relevant sections, as dashed back lines.

If the pointing constraints are tight and the initial RW angular momentum is large, state constrained MPC will need to be used. Unfortunately, the results in [8] do not apply to this type of OCP. In practice, however, simulations show that, for soft constraints at least, implementations that rely on a reduced number of iterations still provide acceptable closed-loop responses. In Figure 9 RW desaturation from the same IC as in Figure 2 is considered with identical input constraints. Soft constraints on the angles are imposed: all must remain within $10^{\circ} \approx 0.17$ [rad] of the nominal position. The optimal solution using the Fischer–Burmeister solver (FBRS) from [15] (dashed lines) and one obtained by limiting the FBRS solver to a maximum of 3 iterations per time step and using warm-starting (solid lines) are presented.

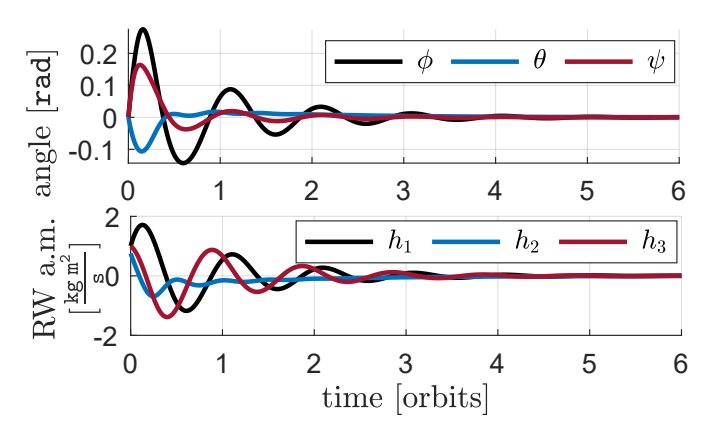


Fig. 8: TDMPC (l=1) controlled nonlinear spacecraft desaturation maneuver with state constraints active: the amplitude of ϕ , θ , ψ must remain smaller than 0.4 [rad].

In both cases desaturation is achieved. When comparing with the unconstrained case (Figure 2), the suboptimal solution is able to keep the constraint exceedances small. The time required for desaturation is smaller than 8 orbits. Notably, limiting the number of iterations to less than 3 leads to significant constraint violation.

V. CONCLUSION

The Time Distributed MPC (TDMPC) with a small number of iterations per time step can successfully achieve spacecraft attitude stabilization with the concurrent spacecraft reaction wheel desaturation while exploiting the gravity gradient torques and satisfying control constraints. In fact, the results indicate that one iteration per time step of TDMPC is sufficient despite the fact that the coupled spacecraft attitudereaction wheel dynamics are nonlinear and relatively high order. The developed in recent publications procedures for estimating the required number of iterations and constraint admissible closed-loop regions of attraction can be exploited for this application, and their use has been illustrated in several case studies. Future work will be directed towards less conservative handling of state constraints on spacecraft attitude and to treating desaturation of reaction wheel arrays with more than three reaction wheels.

REFERENCES

- D. Liao-McPherson, M. M. Nicotra, and I. Kolmanovsky, "Timedistributed optimization for real-time model predictive control: Stability, robustness, and constraint satisfaction," *Automatica*, vol. 117, p. 108973, 2020.
- [2] A. E. Bryson, Control of Spacecraft and Aircraft. Princeton university press Princeton, New Jersey, 1993, vol. 41.
- [3] J. B. Rawlings, D. Q. Mayne, and M. Diehl, Model Predictive Control: Theory, Computation, and Design. Nob Hill Publishing Madison, WI, 2017, vol. 2.
- [4] Ø. Hegrenæs, J. T. Gravdahl, and P. Tøndel, "Spacecraft attitude control using explicit model predictive control," *Automatica*, vol. 41, no. 12, pp. 2107–2114, 2005.
- [5] A. Guiggiani, I. Kolmanovsky, P. Patrinos, and A. Bemporad, "Constrained model predictive control of spacecraft attitude with reaction wheels desaturation," in 2015 European Control Conference (ECC), 2015, pp. 1382–1387.

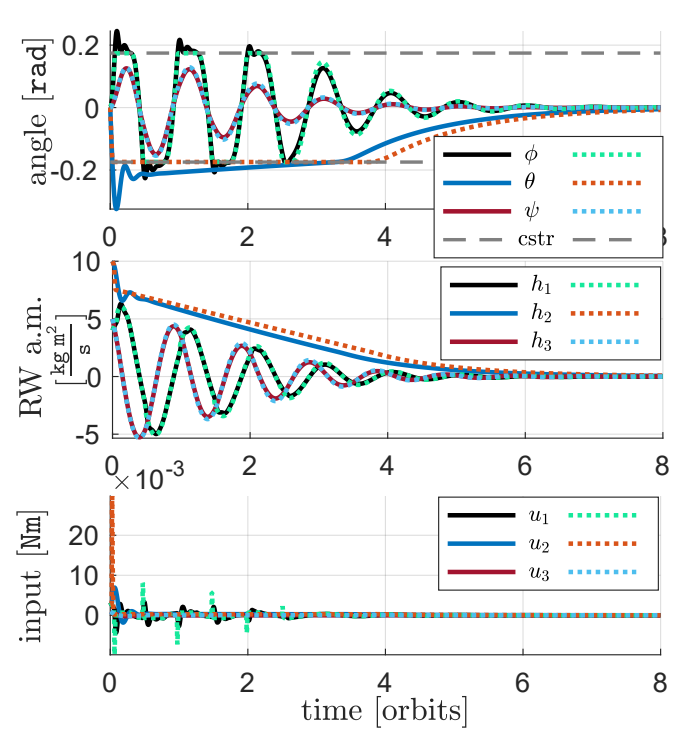


Fig. 9: State evolution for the spacecraft desaturation maneuver subject to pointing constraints (angles within 0.17 [rad] of nominal value). Use of a state constrained MPC [15]. Two cases are presented the optimal solution (dashed lines) and a suboptimal solution computed using a maximum of 3 iterations per time step (solid lines).

- [6] M. Diehl, R. Findeisen, F. Allgöwer, H. G. Bock, and J. P. Schlöder, "Nominal stability of real-time iteration scheme for nonlinear model predictive control," *IEE Proceedings-Control Theory and Applications*, vol. 152, no. 3, pp. 296–308, 2005.
- [7] D. Liao-McPherson, T. Skibik, J. Leung, I. V. Kolmanovsky, and M. M. Nicotra, "An analysis of closed-loop stability for linear model predictive control based on time-distributed optimizat ion," *IEEE Transactions on Automatic Control*, 2021.
- [8] J. Leung, D. Liao-McPherson, and I. V. Kolmanovsky, "A computable plant-optimizer region of attraction estimate for time-distributed linear model predictive control," in 2021 American Control Conference (ACC), 2021, pp. 3384–3391.
- [9] A. Alessio and A. Bemporad, "A survey on explicit model predictive control," in *Nonlinear Model Predictive Control*. Springer, 2009, pp. 345–369.
- [10] B. Wie, Space Vehicle Dynamics and Control. Aiaa, 1998.
- 11] D. Q. Mayne, J. B. Rawlings, C. V. Rao, and P. O. Scokaert, "Constrained model predictive control: Stability and optimality," *Automatica*, vol. 36, no. 6, pp. 789–814, 2000.
- [12] D. Limón, T. Alamo, F. Salas, and E. F. Camacho, "On the stability of constrained mpc without terminal constraint," *IEEE transactions on automatic control*, vol. 51, no. 5, pp. 832–836, 2006.
- [13] MATLAB, version 9.12.0 (R2012a). Natick, Massachusetts: The MathWorks Inc., 2022.
- [14] M. M. Nicotra and E. Garone, "The explicit reference governor: A general framework for the closed-form control of constrained nonlinear systems," *IEEE Control Systems Magazine*, vol. 38, no. 4, pp. 89–107, 2018
- [15] D. Liao-McPherson, M. Huang, and I. Kolmanovsky, "A regularized and smoothed Fischer–Burmeister method for quadratic programming with applications to model predictive control," *IEEE Transactions on Automatic Control*, vol. 64, no. 7, pp. 2937–2944, 2018.